Effects of ghost dark energy perturbations on the evolution of spherical overdensities

Mohammad Malekjani,[1]⋆ Tayebe Naderi[1] and Francesco Pace[2]

[1]*Department of Physics, Bu-Ali Sina University, Hamedan 65178, Iran*
[2]*Jodrell Bank Centre for Astrophysics, School of Physics and Astronomy, The University of Manchester, Manchester M13 9PL, UK*

ABSTRACT

While in the standard cosmological model the accelerated expansion of the Universe is explained by invoking the presence of the cosmological constant term, it is still unclear the true origin of this stunning observational fact. It is therefore interesting to explore alternatives to the simplest scenario, in particular by assuming a more general framework where the fluid responsible for the accelerated expansion is characterized by a time-dependent equation of state. Usually these models, dubbed dark energy models, are purely phenomenological, but in this work we concentrate on a theoretically justified model, the ghost dark energy model. Within the framework of the spherical collapse model, we evaluate effects of dark energy perturbations both at the linear and non-linear level and transfer these results into an observable quantity, the mass function, by speculatively taking into account contributions of dark energy to the mass of the haloes. We showed that the growth rate is higher in ghost models and that perturbations enhance the number of structures with respect to the Λ cold dark matter model, with stronger effects when the total mass takes into account dark energy clumps.

Key words: cosmology: theory – dark energy – large-scale structure of Universe.

1 INTRODUCTION

In the standard cosmological model, the small initial fluctuations that were seeded during the phase of inflationary expansion, some 10^{-35} s after the big bang, are the origin of the large-scale structures (LSS) that we observe today, i.e. galaxies and clusters of galaxies (Starobinsky 1980; Guth 1981; Linde 1990). Subsequently, these fluctuations grew under the influence of gravitational collapse (Gunn & Gott 1972; Press & Schechter 1974; White & Rees 1978; Peebles 1993; Peacock 1999; Sheth & Tormen 1999; Barkana & Loeb 2001; Peebles & Ratra 2003; Ciardi & Ferrara 2005; Bromm & Yoshida 2011). Most of the growth has taken place after the decoupling of photons and electrons. The spherical collapse model (SCM) introduced by Gunn & Gott (1972) is a simple analytical model to study the evolution of the growth of cosmic structures. The scales of interest in the SCM are much smaller than the Hubble length and the velocities are non-relativistic. Therefore, pseudo-Newtonian gravity can be used to study the evolution of the overdensities. With pseudo-Newtonian gravity we refer to the fact that it is possible to use Newton's hydrodynamical equations in an expanding Universe including relativistic contributions to the Poisson equation, i.e. the contribution of pressure terms. At early times, when the overdensities are small, linear theory is able to follow the evolution of spherical overdense regions. In this phase, due to self-gravity, the overdense region expands at a slower rate compared to the Hubble flow. At a particular scalefactor, depending on the particular background history, the spherical region reaches a maximum radius and completely detaches from the background expansion. This is the so-called turn-around epoch. Subsequently, the collapse proceeds under the overdense region own gravity and the system reaches a final steady state with a specific radius due to virialization processes. The dynamics of the SCM depends strongly on the evolution of the background Hubble flow. The SCM was extended and improved in several works (Fillmore & Goldreich 1984; Bertschinger 1985; Hoffman & Shaham 1985; Ryden & Gunn 1987; Avila-Reese, Firmani & Hernández 1998; Subramanian, Cen & Ostriker 2000; Ascasibar et al. 2004; Williams, Babul & Dalcanton 2004). More recently, this formalism has been extended to include shear and rotation terms (Del Popolo, Pace & Lima 2013a,c; Del Popolo et al. 2013b) and non-minimally coupled models (Pace et al. 2014a).

On the other hand, recent developments in observational cosmology using high-quality data including Type Ia supernovae (SNe Ia), cosmic microwave background (CMB), baryonic acoustic oscillations (BAO) and LSS, converge to a standard cosmological model in a spatially flat geometry with a cosmic dark sector usually in the form of pressureless cold dark matter (CDM) and dark energy (DE) with negative pressure, respectively, in order to interpret the observed flat rotation curves of spiral galaxies and the

⋆ E-mail: malekjani@basu.ac.ir

accelerated expansion of the Universe (Riess et al. 1998, 2004, 2007; Perlmutter et al. 1999; Jaffe et al. 2001; Tegmark et al. 2004; Eisenstein et al. 2005; Ho et al. 2008; Percival et al. 2010; Jarosik et al. 2011; Komatsu et al. 2011; Planck Collaboration XV 2014; Planck Collaboration XVI 2014). On the basis of the *Planck* experiment results (Planck Collaboration XVI 2014), DE amounts to ∼68 per cent, CDM and usual baryons to ∼27 per cent and ∼5 per cent of the total energy budget of the Universe, respectively.

Einstein's cosmological constant Λ with time-independent equation-of-state (EoS) parameter $w_\Lambda = -1$ is the first and simplest candidate to describe DE. Although Λ is the simplest model, it suffers from severe theoretical and conceptual problems: the fine tuning and the cosmic coincidence problems (Weinberg 1989; Sahni & Starobinsky 2000; Carroll 2001; Padmanabhan 2003; Peebles & Ratra 2003; Copeland, Sami & Tsujikawa 2006). Moreover since Λ is constant in space and time, it does not cluster and has a negligible contribution to the energy density budget of the Universe at high redshifts, so that it affects the evolution of structures in the Universe at $z \leq 1$.

In order to solve or at least alleviate the theoretical problems of the ΛCDM Universe, a wealth of dynamical DE models with a time varying EoS parameter $w_{\rm de}(z)$ has been proposed. Scalar fields models including quintessence (Ratra & Peebles 1988; Wetterich 1988), phantom (Caldwell 2002; Nojiri & Odintsov 2003a,b), k-essence (Armendariz-Picon, Mukhanov & Steinhardt 2000; Chiba, Okabe & Yamaguchi 2000), tachyon (Padmanabhan 2002; Sen 2002) and dilaton (Gasperini, Piazza & Veneziano 2002; Arkani-Hamed et al. 2004; Piazza & Tsujikawa 2004) are few examples of such dynamical DE models which have been discussed extensively in literature.

Other dynamical DE models which can successfully interpret the current accelerating Universe are constructed on the basis of quantum gravity theories. Models such as holographic dark energy (HDE) models (Hořava & Minic 2000; Thomas 2002) and age-graphic dark energy (ADE) models (Cai 2007) are derived in the framework of quantum gravity, by introducing a new degree of freedom or by modifying the theory of gravity (Hořava & Minic 2000; Thomas 2002; Cai 2007). Recently, ghost DE models have attracted a lot of interests in the category of dynamical DE models (see Section 2 for a in depth description of this class of models).

Dynamical DE models not only alleviate the theoretical problems affecting the cosmological constant Λ, but also, like pressureless matter, possess fluctuations. Hence, these models directly affect:

(i) the dynamics of the background cosmology through the modification of the Hubble parameter;

(ii) the matter power spectrum and large-scale clustering via their fluctuations.

These two parameters are important and give a significant influence to DE perturbations on the matter power spectrum and large-scale structure formation. The first is that the EoS parameter of DE should be different from -1. The second is the effective sound speed $c_{\rm e}^2$ which connects the density and pressure perturbations according to $\delta p = c_{\rm e}^2 \delta\rho$. In fact, the sound horizon of DE is given by $c_{\rm s}H^{-1}$. DE can cluster only on scales larger than the sound horizon and smaller than the gravitational horizon, $c_{\rm e}H^{-1} < \lambda < H^{-1}$. Here, we consider two different cases (in units of the speed of light, c) usually discussed in literature: $c_{\rm e}^2 = 1$ (smooth DE) and $c_{\rm e}^2 = 0$ (clustering DE). In the first case, the sound horizon of DE is equal to the Hubble length, so that DE perturbations occur on scales equal to or larger than the Hubble horizon and are therefore negligible on sub-Horizon scales. In the second scenario, the sound speed is very small compared to the speed of light c. Therefore, the sound hori-

zon of DE is significantly smaller than the Hubble horizon. In this case, one can consider DE perturbations with a wavelength larger than the sound horizon and smaller than the gravitational Hubble horizon which can grow in a similar fashion to matter perturbations which growth under gravitational instability (Armendariz-Picon, Mukhanov & Steinhardt 2001; Abramo, Batista & Rosenfeld 2009a; Appleby, Linder & Weller 2013; Pace, Batista & Del Popolo 2014b; Mehrabi, Malekjani & Pace 2015).

The SCM has been investigated and improved in clustering DE models in order to study how DE perturbations impact structure formation in the highly non-linear regime (Abramo et al. 2007, 2009b; Pace et al. 2014a,b). In this work, we extend the SCM in ghost DE models by taking into account the perturbations of the DE fluid. We study the evolution of overdensities in ghost DE models and obtain the linear overdensity threshold for collapse $\delta_{\rm c}$ as well as the virial overdensity $\Delta_{\rm vir}$ parameters. We show how these quantities are affected by DE clustering in ghost DE models. We then follow the SCM in clustering ghost DE Universes by calculating the mass function and the cluster number count with the Press–Schechter formalism.

The paper is organized as follows. In Section 2, we introduce the ghost DE models and describe the evolution of background cosmology in these models. In Section 3, the non-linear SCM in clustering ghost DE models is presented. In Section 4, we compute the predicted mass function and cluster number count in ghost DE models using the Press–Schechter formalism by taking into account the clustering DE sector. Finally, we conclude and summarize our results in Section 5.

2 BACKGROUND COSMOLOGY IN GHOST DE MODELS

The origin of ghost fields traces back to Veneziano ghosts which have been proposed to find a solution to the $U(1)$ problem in the low-energy effective QCD theory (Veneziano 1979; Witten 1979; Kawarabayashi & Ohta 1980; Rosenzweig, Schechter & Trahern 1980). Although in this formalism, the ghost field has no contribution in the flat Minkowski space–time, in curved space–time it has a small energy density proportional to $\Lambda_{\rm QCD}^3 H$, where H is the Hubble parameter and $\Lambda_{\rm QCD}^3$ is the QCD mass scale (Ohta 2011). With $\Lambda_{\rm QCD} \sim 100$ MeV and $H \sim 10^{-33}$ eV, the quantity $\Lambda_{\rm QCD}^3 H$ gives the right order of magnitude of the observed energy density of DE ($\sim 3 \times 10^{-3}$eV^4; Ohta 2011). This small vacuum energy density can be considered as a driver engine for the evolution of the Universe. Comparing with other theoretical dynamical DE models like HDE and ADE models in which one should introduce a new parameter or a new degree of freedom, the most important advantage of ghost DE models is that they come from the standard model of particle physics and are totally embedded both in the standard model and in general relativity without introducing any new parameter or new degrees of freedom. This numerical coincidence also shows that this model can solve the fine-tuning problem (Urban & Zhitnitsky 2009b,a, 2010a,b). As it was mentioned above, the energy density in ghost DE model is proportional to the Hubble parameter (Ohta 2011):

$$\rho_{\rm de} = \alpha H, \tag{1}$$

where $\alpha > 0$ is roughly of order $\Lambda_{\rm QCD}^3$. From the observational point of view, ghost DE models can fit a whole set of cosmological data including SNe Ia, BAO, CMB, big bang nucleosynthesis (BBN) and Hubble parameter data (Cai et al. 2011). The cosmological evolution of the models has been investigated in (Urban &

Zhitnitsky 2009b,a, 2010a,b; Rozas-Fernández 2012) who stated that the Universe begins to accelerate at redshift around $z \sim 0.6$.

The Friedmann equation for a Universe containing pressureless dust matter and DE in a flat geometry described by a Friedmann–Robertson–Walker (FRW) metric is given by

$$H^2 = \frac{8\pi G}{3}(\rho_{\mathrm{m}} + \rho_{\mathrm{de}}), \tag{2}$$

where ρ_{m} and ρ_{de} are the energy density of the pressureless dust matter and DE components, respectively, and H is the Hubble parameter. We use equation (1) for the energy density of the DE component and insert it into equation (2) in order to obtain the Hubble parameter in ghost DE cosmologies:

$$H = \frac{4\pi G}{3}\alpha + \sqrt{\left(\frac{4\pi G}{3}\alpha\right)^2 + \frac{8\pi G}{3}\rho_{\mathrm{m}0}a^{-3}}. \tag{3}$$

In terms of the dimensionless energy density $\Omega_{\mathrm{m},0} = 8\pi G\rho_{\mathrm{m},0}/(3H_0^2)$ and redshift parameter $z = 1/a - 1$, the above Hubble equation becomes

$$H(z) = H_0 \left(\kappa + \sqrt{\kappa^2 + \Omega_{\mathrm{m},0}(1+z)^3}\right), \tag{4}$$

where $\kappa = (1 - \Omega_{\mathrm{m},0})/2$.

In the above-mentioned studies, the energy density of ghost DE is assumed to be proportional to the Hubble parameter via equation (1). However, the energy density of the Veneziano ghost field in QCD theory is generally of the form $H + O(H^2)$ (Zhitnitsky 2011). Although in ghost DE models only the leading term H was assumed, it has been shown that the sub-leading term H^2 can also be important in the early evolution of the Universe (Maggiore et al. 2011). A ghost DE model with sub-leading term H^2 is usually called generalized ghost DE model. Cai et al. (2012) showed that generalized ghost DE models result in better agreement with observations compared to ordinary ghost DE models. The energy density of a generalized ghost DE model is given by (Cai et al. 2011)

$$\rho_{\mathrm{de}} = \alpha H + \beta H^2, \tag{5}$$

where α and β are the constants of the model. Inserting equation (5) into equation (2), the Hubble parameter becomes

$$H = \frac{4\pi G}{3\gamma}\alpha + \sqrt{\left(\frac{4\pi G}{3\gamma}\alpha\right)^2 + \frac{8\pi G}{3\gamma}\rho_{\mathrm{m}0}a^{-3}}, \tag{6}$$

where $\gamma = 1 - 8\pi G\beta/3$. Setting $\gamma = 1$, generalized ghost DE model reduces to ordinary ghost DE model ($\beta = 0$), as expected. In terms of the dimensionless matter energy density $\Omega_{\mathrm{m},0}$ and redshift parameter z, the Hubble equation in generalized ghost DE models is given by

$$H(z) = H_0 \left(\kappa + \sqrt{\kappa^2 + \frac{\Omega_{\mathrm{m},0}(1+z)^3}{\gamma}}\right), \tag{7}$$

where $\kappa = (1 - \Omega_{\mathrm{m},0}/\gamma)/2$.

The conservation equations for pressureless dust matter and DE at the background level are

$$\dot{\rho}_{\mathrm{m}} + 3H\rho_{\mathrm{m}} = 0, \tag{8}$$

$$\dot{\rho}_{\mathrm{de}} + 3H(1 + w_{\mathrm{de}})\rho_{\mathrm{de}} = 0, \tag{9}$$

where the dot is the derivative with respect to cosmic time and w_{de} is the DE EoS parameter.

Taking the time derivative of Friedmann equation (2) and using equations (8) and (9) as well as the critical density $\rho_{\mathrm{c}} = 3H^2/(8\pi G)$, we obtain

$$\frac{\dot{H}}{H^2} = -\frac{3}{2}(1 + \Omega_{\mathrm{de}}w_{\mathrm{de}}), \tag{10}$$

where Ω_{de} is the dimensionless density parameter of the DE component. Differentiating equations (1) and (5) with respect to time and inserting the results in the conservation equation for DE (equation 9) and also using equation (10), the EoS parameter for ghost DE and generalized ghost DE models are

$$w_{\mathrm{de}}(z) = \frac{1}{\Omega_{\mathrm{de}}(z) - 2}, \tag{11}$$

$$w_{\mathrm{de}}(z) = \frac{1 - \Omega_{\mathrm{de}}(z) - \gamma}{\Omega_{\mathrm{de}}(z)(1 - \Omega_{\mathrm{de}}(z) + \gamma)}. \tag{12}$$

Setting $\gamma = 1$, equation (12) reduces to (11) as expected. We now calculate the equation of motion for the energy density of DE in ghost DE and generalized ghost DE models. Taking the time derivative of $\Omega_{\mathrm{de}} = \rho_{\mathrm{de}}/\rho_{\mathrm{c}}$ and using equations (1) and (10) and finally changing the time derivative to a derivative with respect to cosmic redshift z, we have

$$\frac{\mathrm{d}\Omega_{\mathrm{de}}(z)}{\mathrm{d}z} = -\frac{3\Omega_{\mathrm{de}}(z)}{2(1+z)}[1 + \Omega_{\mathrm{de}}(z)w_{\mathrm{de}}(z)], \tag{13}$$

for both ghost and generalized ghost DE cosmologies. We see that the evolution of the DE density in ghost DE cosmologies via equation (13) depends on the EoS parameter of the models according to the relations (11) and (12). We solve the system of coupled equations (4), (11), (13) and (7), (12), (13) in order to calculate the evolution of the Hubble and EoS parameters as well as the energy density of DE in ghost and generalized ghost DE cosmologies, respectively. To fix the cosmology, the present values of matter density and DE density parameters are chosen as: $\Omega_{\mathrm{m},0} = 0.27$ and $\Omega_{\mathrm{de},0} = 0.73$ in a spatially flat Universe. The present Hubble parameter is $H_0 = 70$ km s^{-1} Mpc^{-1}.

In Fig. 1, we show the evolution of the EoS parameter w_{de} (top panel), dimensionless Hubble parameter $E = H/H_0$ (middle panel) and energy density of DE component Ω_{de} (bottom panel) as a function of the cosmic redshift z for different ghost, generalized ghost DE and ΛCDM cosmological models. In the case of the generalized ghost DE model, we choose the model parameter γ as 0.96 and 0.90. In all the figures of this work we indicate the ghost DE as GDE and the generalized ghost DE as GGDE. We see that the EoS parameter for ghost and generalized ghost DE models is always bigger than $w_{\Lambda} = -1$ and remains in the quintessence regime, i.e. $w_{\mathrm{de}} > -1$. The Hubble parameter and the DE density are bigger in these models compared to the concordance ΛCDM Universe. This means that the rate of acceleration is stronger for (generalized) ghost models and that the relevance of the DE fluid is important for a longer period of the cosmic history.

3 SPHERICAL COLLAPSE IN GHOST DE COSMOLOGIES

In this section, we investigate the SCM in the framework of clustering ghost and generalized ghost DE cosmologies. The effects of DE perturbations on the evolution of matter overdensities have been extensively investigated in literature (see i.e. Mota & van de Bruck 2004; Abramo et al. 2007, 2008; Abramo et al. 2009a; Creminelli et al. 2010; Basse, Eggers Bjælde & Wong 2011; Batista & Pace
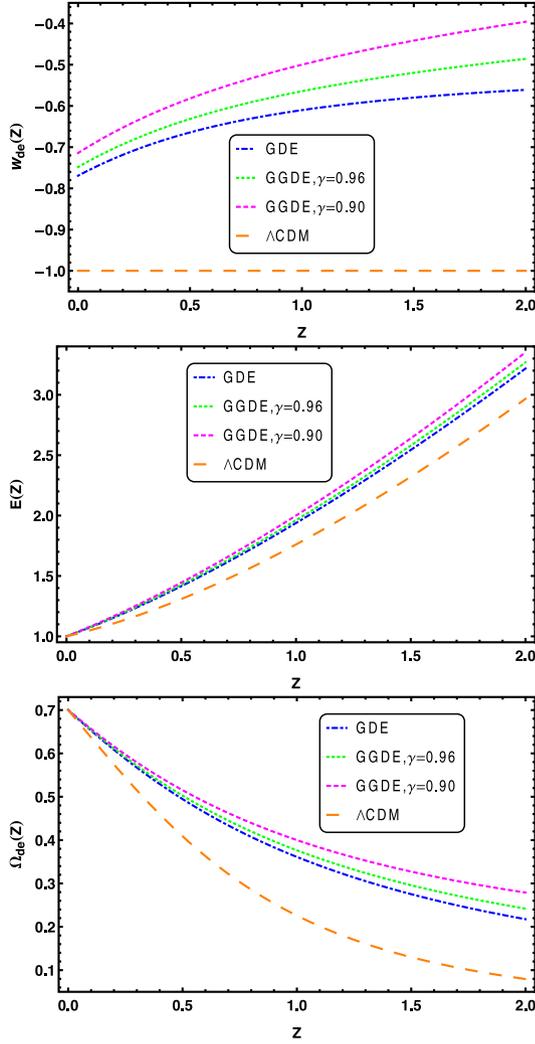
Figure 1. Top panel: evolution of the EoS parameter w_{de}. Middle panel: dimensionless Hubble parameter $E(z)$. Bottom panel: DE density parameter Ω_{de} as a function of cosmic redshift z for the different cosmological models considered in this work. As shown in the legend, the ghost DE is indicated by GDE, generalized ghost DE by GGDE. The ΛCDM model is shown with the orange dashed line, the GDE model with the red short-dashed line and the GGDE model with the brown (pink) short-dashed line for $\gamma = 0.96$ ($\gamma = 0.90$), respectively.

2013; Pace et al. 2014a,b). Following Pace et al. (2014a), the fully perturbed equations for the evolution of non-relativistic dust matter δ_m and DE δ_{de} perturbations in the non-linear regime (without the contribution of shear and rotation) are given by

$$\delta'_m + (1 + \delta_m)\frac{\tilde{\theta}}{a} = 0, \tag{14}$$

$$\delta'_{de} - \frac{3}{a}w_{de}\delta_{de} + [1 + w_{de} + \delta_{de}]\frac{\tilde{\theta}}{a} = 0, \tag{15}$$

$$\tilde{\theta}' + \left(\frac{2}{a} + \frac{E'}{E}\right)\tilde{\theta} + \frac{\tilde{\theta}^2}{3a} + \frac{3}{2a}[\Omega_{DM}\delta_m + \Omega_{de}\delta_{de}] = 0, \tag{16}$$

where $\tilde{\theta} = \theta/H$ is the dimensionless divergence of the comoving peculiar velocity for dust matter and DE.

The linear evolution of overdensities at early times is

$$\delta'_m + \frac{\tilde{\theta}}{a} = 0, \tag{17}$$

$$\delta'_{de} - \frac{3}{a}w_{de}\delta_{de} + [1 + w_{de}]\frac{\tilde{\theta}}{a} = 0, \tag{18}$$

$$\tilde{\theta}' + \left(\frac{2}{a} + \frac{E'}{E}\right)\tilde{\theta} + \frac{3}{2a}[\Omega_{DM}\delta_m + \Omega_{de}\delta_{de}] = 0. \tag{19}$$

As in Pace et al. (2014a,b), to determine the initial conditions to solve the above differential equations describing the evolution of perturbations, we find the initial value $\delta_{m,i}$ such that at the collapse scale factor a_c the matter overdensity diverges, $\delta_m \to \infty$. The initial values for the DE overdensity $\delta_{de,i}$ and peculiar velocity perturbation $\tilde{\theta}_i$ are related to $\delta_{m,i}$ via (Batista & Pace 2013; Pace et al. 2014b):

$$\delta_{de,i} = \frac{n}{(n - 3w)}(1 + w_{de})\delta_{m,i}, \tag{20}$$

$$\tilde{\theta}_i = -n\delta_{m,i}. \tag{21}$$

In the case of an EdS model $n = 1$. However, in DE cosmologies it has been shown that there is a small deviation from unity (Ferreira & Joyce 1998; Batista & Pace 2013). In the limiting case of non-clustering DE models ($c_e = 1$) the coupled non-linear equations (14, 15, 16) and system of linear equations (17, 18, 19), respectively, reduce to the following equations:

$$\delta''_m + \left(\frac{3}{a} + \frac{E'}{E}\right)\delta'_m - \frac{4}{3}\frac{\delta'^2_m}{1 + \delta_m} - \frac{3\Omega_{m0}}{2a^5E^2}\delta_m(1 + \delta_m) = 0, \tag{22}$$

$$\delta''_m + \left(\frac{3}{a} + \frac{E'}{E}\right)\delta'_m - \frac{3\Omega_{m0}}{2a^5E^2}\delta_m = 0, \tag{23}$$

as expected (see also Pace, Waizmann & Bartelmann 2010). In the case of non-clustering ghost and generalized ghost DE models, we will solve equations (22, 23), instead of the previous ones.

4 RESULTS

We first solve the system of equations (17), (18), (19) for the case of clustering DE ($c_e = 0$) and (23) for non-clustering DE ($c_e = 1$) in order to determine the linear evolution of the overdensities δ_m and δ_{de} (δ_m in the non-clustering DE case) and obtain the linear growth factor $D_+(z) = \delta_m(z)/\delta_m(z = 0)$ as a function of cosmic redshift z for the different cosmological models considered in this work.

In Fig. 2, the evolution of the growth factor normalized at $z = 0$ and divided by the scale factor a is presented as a function of redshift. In the EdS model (black solid line) D_+/a is equal to 1 at any time showing that the growth of matter perturbations δ_m is the same at all redshifts. In a ΛCDM Universe (orange long-dashed curve) the growth factor is higher than the EdS model throughout its history, but falls for lower redshifts. The lowering of the growth factor at lower redshifts is due to the fact that at late times the cosmological constant dominates the energy budget of the Universe and suppresses the amplitude of perturbations. On the other hand, a larger growth factor in a ΛCDM Universe at higher redshift shows that the growth of dust matter perturbations will be stronger than in a EdS Universe at early times. For ghost and generalized ghost DE models we show D_+/a for two extreme cases: fully clustering DE ($c_e = 0$) and homogeneous DE ($c_e = 1$) models. In the case
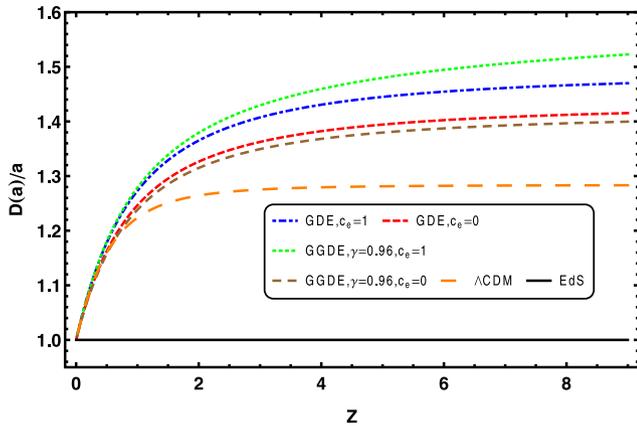
Figure 2. Time evolution of the growth factor normalized to the present time and divided by the scale factor a as a function of the cosmic redshift z for different cosmological models. Black solid line shows the EdS model, the orange long-dashed line the ΛCDM model, the blue (green) dot–dashed (dotted) line the homogeneous ghost (generalized ghost) DE model, while the red (brown) dashed line the clustering ghost (generalized ghost) DE cosmology.

Figure 3. The variation of the linear threshold density contrast δ_c as a function of the collapse redshift for the different cosmological models analysed in this work. Line styles and colours are as in Fig. 2.

of generalized ghost DE model, we choose a value of 0.96 for the model parameter γ. The red and brown dashed curves stand for clustering ghost and generalized ghost DE models, respectively. The blue dot–dashed and green dotted curves show the variation of D_+/a for homogeneous ghost and generalized ghost DE Universes, respectively. We see that the growth factor is largest (intermediate) for homogeneous (clustering) ghost and generalized ghost DE models compared to the concordance ΛCDM Universe. It is worth to mention that D_+/a changes more rapidly at low redshifts where DE dominates the energy budget of the Universe. At early times instead, the relative change is much shallower. Differences are obviously still noticeable in the models. In particular, we notice that while D_+/a for the ΛCDM model is almost a constant, this is not entirely the case for the DE models analysed in this work. This is easily interpreted taking into account the stronger importance of DE at early times, as clearly shown in the lower panel of Fig. 1. Similarly to the ΛCDM Universe, in ghost and generalized ghost DE models, DE suppresses the growth of perturbations at low redshifts. More quantitatively, at high redshifts, the growth of perturbations parameter D_+/a in non-clustering (clustering) generalized ghost DE model is ≈18.7 per cent (≈10.9 per cent) larger than in the ΛCDM concordance model. These values are only mildly larger than the ghost DE models, where D_+/a differs of ≈14.5 per cent (≈10 per cent) for non-clustering (clustering) ghost DE models with respect to a ΛCDM model.

4.1 SCM parameters

Here we evaluate the two characterizing quantities of the SCM: the linear overdensity parameter δ_c and the virial overdensity $\Delta_{\rm vir}$ for ghost and generalized ghost DE cosmologies. The linear overdensity δ_c together with the growth factor D_+ is important in order to evaluate the mass function in the Press–Schechter formalism (Press & Schechter 1974; Bond et al. 1991; Sheth & Tormen 2002). The virial overdensity $\Delta_{\rm vir}$ is used to calculate the size of spherically symmetric haloes with given mass M.

We search the initial conditions $\delta_{\rm m,i}$ following the general approach in Pace et al. (2010, 2012) and then we use equations (20) and (21) to determine $\delta_{\rm de,i}$ and $\tilde{\theta}_i$. Once the initial conditions are
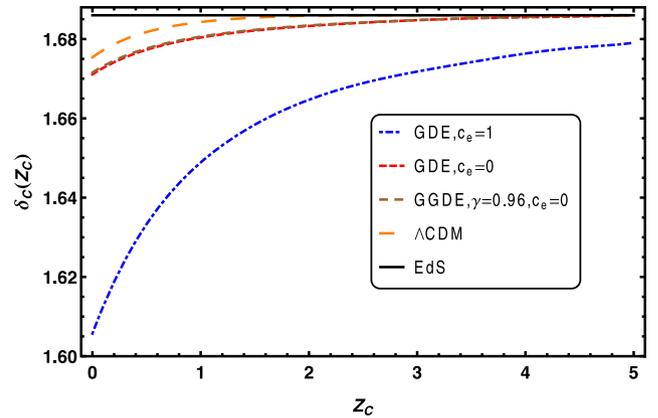
found, we then solve the system of equations (17), (18) and (19) in order to obtain $\delta_c = \delta_m(z = z_c)$. In the non-clustering case, we solve equation (23) to calculate δ_c.

The collapse redshift z_c is defined as the redshift at which the matter overdensity tends to infinity $\delta_m \to \infty$ (see also Pace et al. 2010, 2012, 2014a,b).

In Fig. 3, the evolution of the linear overdensity δ_c as a function of the collapse redshift z_c is presented for different models: EdS, ΛCDM, homogeneous and clustering ghost DE and clustering generalized ghost DE. We refer to the caption for line styles and colours of each model. Analogous to the previous section, we use $\gamma = 0.96$ in the case of generalized ghost DE models. In all DE models, the linear overdensity parameter approaches the fiducial value in the EdS Universe $\delta_c \approx 1.686$ at high enough redshifts, as expected. In fact at high redshifts, the Universe is dominated by pressureless dust matter and the effects of DE on the scenario of structure formation are negligible. At lower redshifts, δ_c decreases and deviates from the EdS limit. The important point to note is that in clustering ghost and generalized ghost DE models, the behaviour of δ_c is more similar to the ΛCDM Universe with respect to the homogeneous models. This result is in agreement with what found by Pace et al. (2010) and Batista & Pace (2013) for early DE models and Pace et al. (2014b) for clustering quintessence and phantom DE models. Quantitatively, we see that the differences between homogeneous ghost and generalized ghost DE models with the ΛCDM model at the present time are roughly 4.5 and 21.5 per cent, respectively, while in the case of clustering ghost and generalized ghost models the differences are very small, of the order of ≈0.25 per cent for both cases. As for the case of perturbations in early DE models, we can explain the fact that perturbations in the DE fluid make the model more similar to the ΛCDM model by taking into account that the Poisson equation is now modified and the gravitational potential is sourced also by DE perturbations.

In the framework of the SCM, the virialization process of pressureless dust matter and the size of forming haloes are strongly affected by the DE sector (Lahav et al. 1991; Wang & Steinhardt 1998; Mota & van de Bruck 2004; Horellou & Berge 2005; Wang & Tegmark 2005) and also its perturbations (Abramo et al. 2007, 2008, 2009a; Batista & Pace 2013; Pace et al. 2014a,b). The virial overdensity is defined as $\Delta_{\rm vir} = \zeta(x/y)^3$, where ζ is the overdensity at the turn-around epoch, x is the scale factor normalized to the turn-around scale factor and y is the ratio between the virialization radius and the turn-around radius (Wang & Steinhardt 1998). In an
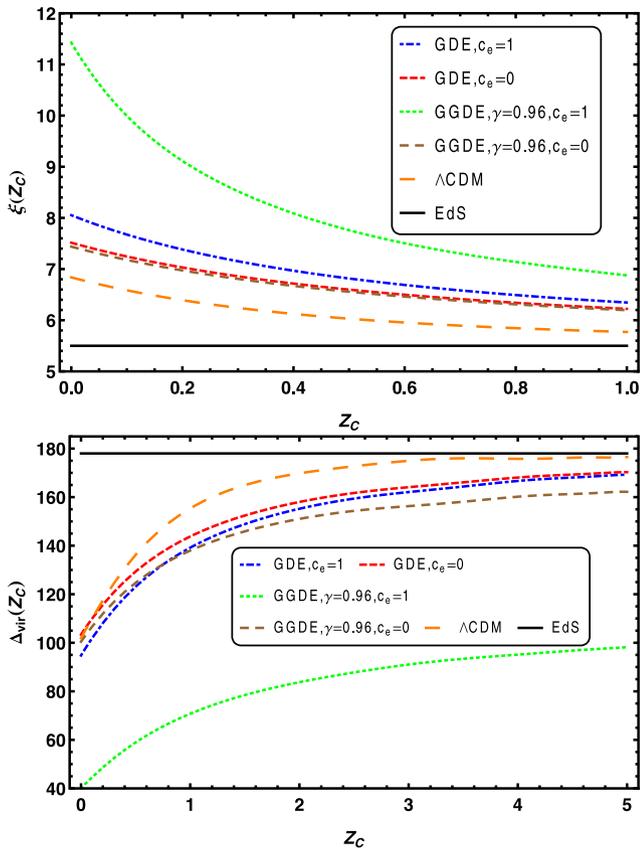
Figure 4. The variation of turn around overdensity ζ (top panel) and virial overdensity $\Delta_{\rm vir}$ (bottom panel) with respect to the collapse redshift z_c for various models considered in this work. Line styles and colours are as in Fig. 2.

EdS cosmology, it is simple to show that $y = 1/2$, $\zeta \approx 5.6$ and $\Delta_{\rm vir} \approx 178$ independently of the cosmic redshift (see also Naderi, Malekjani & Pace 2015). In DE cosmologies, $\Delta_{\rm vir}$ depends on the evolution of the DE fluid and it is a redshift dependent quantity. In particular, according to whether DE takes part or not into the virialization process, the quantity y may be larger or smaller than $1/2$ and the parameter $\Delta_{\rm vir}$ can be affected by the clustering of DE (Maor & Lahav 2005; Pace et al. 2014a,b).

In the line of these studies, we calculate the turn-around and virial overdensities ζ and $\Delta_{\rm vir}$ in ghost and generalized ghost DE cosmologies. We also determine how the clustering of the DE component can change the variation of ζ and $\Delta_{\rm vir}$ in these models. Our results are presented in Fig. 4. In the top panel, the variation of the overdensity at the turn-around redshift ζ is shown for the different DE models investigated in this work. In the limiting case of the EdS model, $\zeta = 5.6$ independently of the cosmic time. At early times, ζ tends to the critical value $\zeta = 5.6$ representing the early matter-dominated era. The value of ζ is larger for both clustering and non-clustering versions of ghost and generalized ghost DE models, compared to the concordance ΛCDM model. Differences between the DE models and the ΛCDM model cover a relatively huge spectrum of values, according to whether we take into account the perturbations of the DE fluid. In particular for homogeneous (generalized) ghost DE models, differences are of the order of (67 per cent) 17 per cent while when perturbations are taken into account, differences drop down to (9 per cent) 10 per cent. This shows how the generalized ghost model, is much more sensitive to the inclusion of DE pertur-

bations. Once again, this is due the higher amount of DE density at earlier time for these kind of models. Hence, we conclude that in the context of ghost DE scenarios the perturbed spherical perturbations detach from the background Hubble flow with higher overdensities compared to the EdS and ΛCDM Universes. We also notice that the results for clustering ghost and generalized ghost DE models are closer to what is found for the reference ΛCDM model compared to the non-clustering case.

In the bottom panel, the results for the virial overdensity $\Delta_{\rm vir}$ are presented. In the case of ghost DE models, the results are closer to the reference ΛCDM model. In these models, the difference between homogeneous and clustering DE is very small. However, in the case of generalized ghost cosmology the differences are more pronounced. Differences between ghost DE models and ΛCDM model at the present time are of the order of 60 per cent for non-clustering generalized ghost DE model and 7 per cent for homogenous ghost DE models, roughly as for the overdensity at the turn-around radius. This is not surprising, since this quantity is the main ingredient used to evaluate the virial overdensity. When perturbations in DE are taken into account differences are only of the order of 1.5 per cent for both classes analysed. These results are similar to what found in Del Popolo et al. (2013c) and Pace et al. (2014b).

4.2 Mass function and halo number density

We know that galaxies and cluster of galaxies are embedded in the extended haloes of CDM. In the Press–Schechter formalism (Press & Schechter 1974), the abundance of CDM haloes can be described as a function of their mass and a Gaussian distribution function expresses the fraction of the volume of the Universe which collapses into an object of mass M at a certain redshift z. In this formalism, the comoving number density of virialized structures with masses in the range of M and $M + {\rm d}M$ at redshift z is given by

$$\frac{{\rm d}n(M, z)}{{\rm d}M} = -\frac{\rho_{\rm m0}}{M} \frac{{\rm d}\ln\sigma(M, z)}{{\rm d}M} f(\sigma),$$ (24)

where σ is the rms of the mass fluctuation in spheres of mass M and $f(\sigma)$ is the mass function. The standard mass function in the Press–Schechter formalism is given by (Press & Schechter 1974)

$$f(\sigma) = \sqrt{\frac{2}{\pi}} \frac{\delta_{\rm c}(z)}{\sigma(M, z)} \exp\left[-\frac{\delta_{\rm c}^2(z)}{2\sigma^2(M, z)}\right].$$ (25)

Although the standard mass function provides a good general representation of the predicted number density of CDM haloes, it deviates from simulations due to an overprediction of low-mass objects and an underprediction of high-mass objects at the present time (Sheth & Tormen 1999, 2002). Here, we use another popular fitting formula proposed by Sheth & Tormen (Sheth & Tormen 1999, 2002), the so-called ST mass function:

$$f_{\rm ST}(\sigma) = A\sqrt{\frac{2a}{\pi}} \left[1 + \left(\frac{\sigma^2(M, z)}{a\delta_{\rm c}^2(z)}\right)^p\right] \frac{\delta_{\rm c}(z)}{\sigma(M, z)}$$

$$\times \exp\left(-\frac{a\delta_{\rm c}^2(z)}{2\sigma^2(M, z)}\right),$$ (26)

where the numerical parameters are: $A = 0.3222$, $a = 0.707$ and $p = 0.3$. Putting $A = 1/2$, $a = 1$ and $p = 0$, the well-known

Press–Schechter mass function can be recovered as expected. In a Gaussian density field, the mass variance σ^2 is given by

$$\sigma^2 = \frac{1}{2\pi^2} \int_0^\infty k^2 P(k) W^2(kR) \mathrm{d}k, \qquad (27)$$

where $R = (3M/4\pi\rho_{m,0})^{1/3}$ is the radius of the overdense spherical path at the present time, $W(kR) = 3[\sin(kR) - kR\cos(kR)]/(kR)^3$ is the Fourier transform of a spherical top-hat profile window function with radius R and $P(k)$ is the linear power spectrum of density fluctuations (Peebles 1993).

The number density of objects above a given mass at a certain fixed redshift is

$$n(> M) = \int_M^\infty \frac{\mathrm{d}n}{\mathrm{d}M'} \mathrm{d}M'. \qquad (28)$$

In this section, having at hands all the necessary ingredients, we can compute the predicted number density of virialized objects in the Press–Schechter formalism for ghost and generalized ghost DE cosmologies. As first step, we use equation (28) for non-clustering ghost and generalized ghost DE models. In next section, we investigate the predicted number density of virialized clusters on the basis of the formulation presented in Creminelli et al. (2010), Basse et al. (2011) and Batista & Pace (2013) where the total mass of the haloes is affected by DE perturbations.

We use the f_{ST} mass function given in equation (26) and choose four different redshifts: $z = 0, 0.5, 1.0$ and 2.0. In order to calculate σ^2, we follow the formulations presented in Abramo et al. (2007) and Naderi et al. (2015). We also adopt the ΛCDM model as reference model with normalization of the matter power spectrum $\sigma_8 = 0.776$, in agreement with recent observations (Planck Collaboration XVI 2014; Planck Collaboration XX 2014). In Fig. 5, we show the ratio of the number of objects above a given mass M

between the ghost and generalized ghost DE models and the concordance ΛCDM model, in the case of non-clustering DE cosmologies. In the case of generalized ghost DE model, we choose three different values for the model parameter: $\gamma = 0.90, 0.96$ and 0.98. As was discussed in Section (2), for $\gamma = 1.0$, the generalized ghost model reduces to the ghost DE model. In the upper-left (right-hand) panel, the results are presented for redshift $z = 0$ ($z = 0.5$). The lower-left (right-hand) panel is for haloes at redshift $z = 1$ ($z = 2$), as indicated in the legends. Due to the identical normalization of the matter power spectrum, we see that at $z = 0$ all models have the same number of objects. At $z = 0.5$, the ghost ($\gamma = 1$) and generalized ghost with $\gamma = 0.96\ 0.98$ are still giving the same number of object compared to the concordance ΛCDM model, with very small differences for the large mass tail of the distribution ($10^{15}\,M_\odot\,h^{-1}$). However, for smaller values of γ the differences between the generalized ghost and the ΛCDM model are considerable. For $\gamma = 0.90$, the predicted number density for virialized haloes at high-mass tail ($10^{15}\,M_\odot\,h^{-1}$) is roughly 40 per cent lower than the concordance ΛCDM model (see top-right panel of Fig. 5. At higher redshifts, $z = 1$ and 2, the predicted number of structures exceeds what predicted by the ΛCDM model, in the cases of ghost and generalized ghost DE models with model parameter γ close to unity, i.e. $\gamma = 0.96, 0.98$. The generalized ghost model with low value $\gamma = 0.90$ shows a decrement in the number of objects compared to other cases. We see that a major difference between ghost DE models and ΛCDM model takes place at high mass while all models are roughly producing the same number of objects at the low-mass tail, as expected. From a more quantitative point of view, at redshift $z = 1$, the ghost DE model shows an increment in the number of structures of ≈ 47 per cent, while for the generalized ghost DE model with $\gamma = 0.98$ ($\gamma = 0.96$) the increment is ≈ 38 per cent (≈ 29 per cent), when they are compared to the
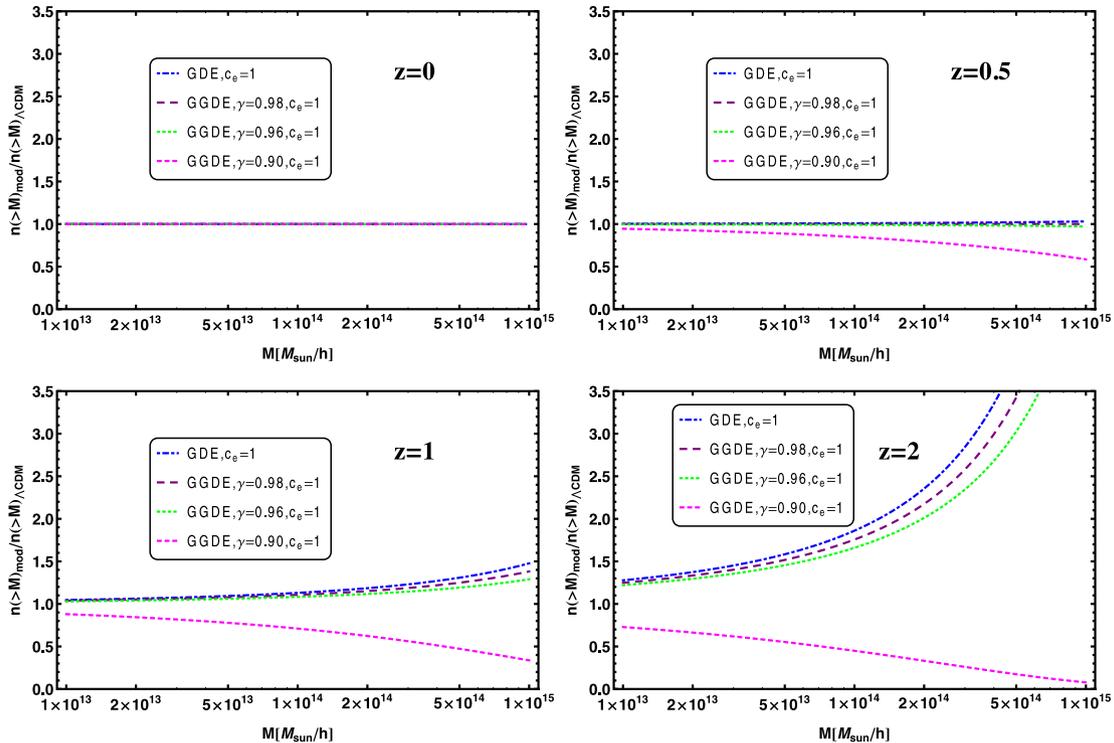

Figure 5. Ratio of the number of objects above a given mass M for haloes at $z = 0$ (top left), $z = 0.5$ (top right), $z = 1.0$ (bottom left) and $z = 2.0$ (bottom right) between the ghost and generalized ghost DE models and the concordance ΛCDM model. The blue dot–dashed curve represents the ghost DE model. The purple dashed, green dotted and pink dashed curves stand for generalized ghost DE model with model parameter $\gamma = 0.98$, $\gamma = 0.96$ and 0.90, respectively.

standard ΛCDM model. Surprisingly, the case with $\gamma = 0.90$ shows a substantial lack of high mass objects, of the order of ≈ 66 per cent for objects of mass $\approx 10^{15}\,\mathrm{M}_\odot\,h^{-1}$.

4.3 Corrected mass function in clustering ghost DE models

It is well known that in EdS cosmology $y = R_{\mathrm{vir}}/R_{\mathrm{ta}} = 1/2$. In the EdS model, the virial overdensity can be calculated analytically and the calculations lead to $\Delta_{\mathrm{vir}} \simeq 178$ independently of the redshift z. It is also well known that this value strongly depends on the particular background cosmology and changes in the presence of DE. It was shown that the virialization process of dark matter overdensities in the non-linear regime depends on the properties of DE models (Lahav et al. 1991; Maor & Lahav 2005; Creminelli et al. 2010; Basse et al. 2011). Moreover, in clustering DE models, we should take into account the contribution of DE perturbations to the total mass of the haloes (Creminelli et al. 2010; Basse et al. 2011; Batista & Pace 2013; Pace et al. 2014a,b). Depending on the quintessence or phantom DE EoS parameter, $w_{\mathrm{de}}(z)$, DE can add or subtract mass to the total mass of the halo, respectively. The fraction of DE mass to be taken into account with respect to the mass of the dark matter is given by the quantity $\epsilon(z) = M_{\mathrm{de}}/M_{\mathrm{m}}$. The mass of dark matter M_{m} is defined as

$$M_{\mathrm{m}} = 4\pi\bar\rho_{\mathrm{m}} \int_0^{R_{\mathrm{vir}}} \mathrm{d}R\, R^2 (1+\delta_{\mathrm{m}}). \tag{29}$$

where $\bar\rho_{\mathrm{m}}$ is the mean density of dark matter. The mass of DE in the virialization process depends on what it is considered to be the mass of the DE component. If we only assume the contribution of DE perturbation, then the mass of the DE component is given by

$$M_{\mathrm{de}}^{\mathrm{P}} = 4\pi\bar\rho_{\mathrm{de}} \int_0^{R_{\mathrm{vir}}} \mathrm{d}R\, R^2 \delta_{\mathrm{de}}\left(1+3c_{\mathrm{e}}^2\right), \tag{30}$$

where $\bar\rho_{\mathrm{de}}$ is the mean density of DE. On the other hand, if we assume also the contribution at the background level (in analogy to dark matter), the total mass of DE is given by

$$M_{\mathrm{de}}^{\mathrm{T}} = 4\pi\bar\rho_{\mathrm{de}} \int_0^{R_{\mathrm{vir}}} R R^2 \left[(1+3w_{\mathrm{de}}) + \delta_{\mathrm{de}}\left(1+3c_{\mathrm{e}}^2\right)\right]. \tag{31}$$

Here, we compute the quantity $\epsilon(z)$ in the case of full clustering DE scenario. It should be noted that due to the background contribution in equation (31), even in the case of homogeneous DE scenarios, DE can add or subtract mass to the dark matter haloes (see also Batista & Pace 2013; Pace et al. 2014a,b). Since we work in the framework of the top-hat spherical profile, the quantities inside the collapsing sphere evolve only in time without any spatial dependence. Hence on the basis of the definition in equation (30), we have

$$\epsilon(z) = \frac{\Omega_{\mathrm{de}}(z)}{\Omega_{\mathrm{m}}(z)} \frac{\delta_{\mathrm{de}}}{1+\delta_{\mathrm{m}}}, \tag{32}$$

and under the same assumption for equation (31)

$$\epsilon(z) = \frac{\Omega_{\mathrm{de}}(z)}{\Omega_{\mathrm{m}}(z)} \frac{1+3w_{\mathrm{de}}(z)+\delta_{\mathrm{de}}}{1+\delta_{\mathrm{m}}}. \tag{33}$$

In Fig. 6 we show the evolution of $\epsilon(z)$ according to equations (32, top panel) and (33, bottom panel) for both ghost and generalized ghost DE models. We refer the reader to the caption for line styles and colours. We notice that according to equation (32), both ghost and generalized ghost DE models give a positive contribution to the total mass of the haloes ($\epsilon(z) > 0$). The quantity ϵ grows with redshift z meaning that the contribution of DE on the total mass is
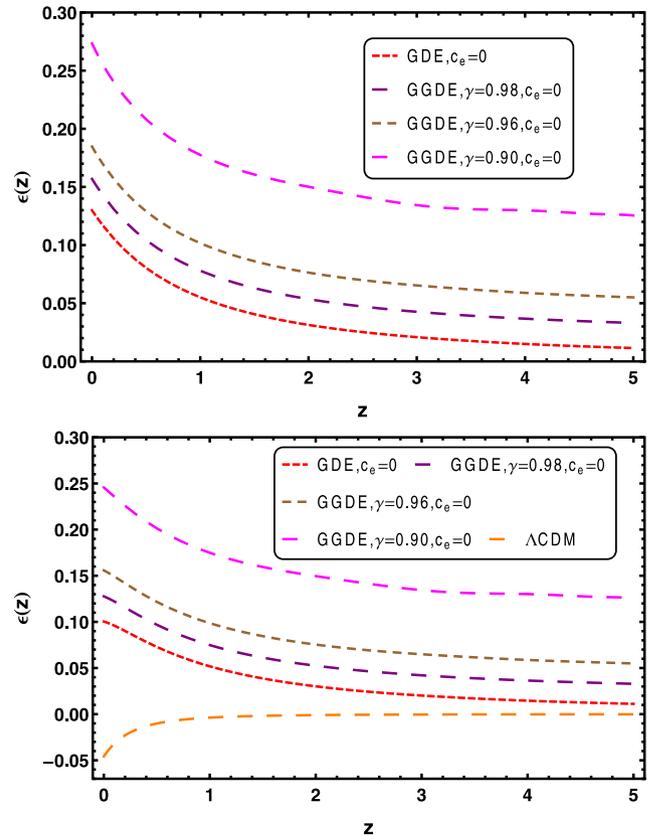

Figure 6. The ratio of DE mass to dark matter mass by using the definition of ϵ via equation (32) in the top panel and equation (33) in the bottom panel. The red dot–dashed curve represents the clustering ghost DE model. The purple long-dashed, brown dashed and pink long-dashed curves stand for clustering generalized ghost DE model with model parameter $\gamma = 0.98$, 0.96 and 0.90, respectively. The orange long-dashed one indicates the ΛCDM model.

larger for haloes which virialize at lower redshifts. This is explained by taking into account the fact that at late times DE perturbations arise, while being negligible at earlier times. In particular, the generalized ghost DE model gives a higher contribution of DE to the total mass of haloes compared to ghost DE model. We also see that a lower value of the model parameter γ results in a higher value of $\epsilon(z)$. On the other hand, using the definition in equation (33), the behaviour of ϵ is different. Looking at equation (33), we see that the sign of the quantity $1+3w_{\mathrm{de}}+\delta_{\mathrm{de}}$ determines how DE contributes to the total mass of the halo. During the history of the halo, when $3w_{\mathrm{de}}+\delta_{\mathrm{de}} < -1$, the contribution of the DE mass is negative and therefore it lowers the total mass of the haloes. The other important point to note is that according to the definition of ϵ via equation (33), one can consider the DE mass even for homogeneous DE models ($\delta_{\mathrm{de}} = 0$). Hence in the bottom panel of Fig. 6 we show ϵ for the ΛCDM model ($w_{\mathrm{de}} = -1$). We also see that for the ΛCDM model ϵ is always negative. On the other hand, when $3w_{\mathrm{de}}+\delta_{\mathrm{de}} > -1$, the contribution of DE is positive. This is the behaviour taking place for ghost and generalized ghost DE models. Comparing the top and bottom panels in Fig. 6, we see that for ghost and generalized DE models the values of ϵ according to the second definition are lower than equation (32).

We now compute the number density of virialized haloes in the presence of DE mass correction. Following the procedure outlined in Batista & Pace (2013) and Pace et al. (2014a), in the presence of
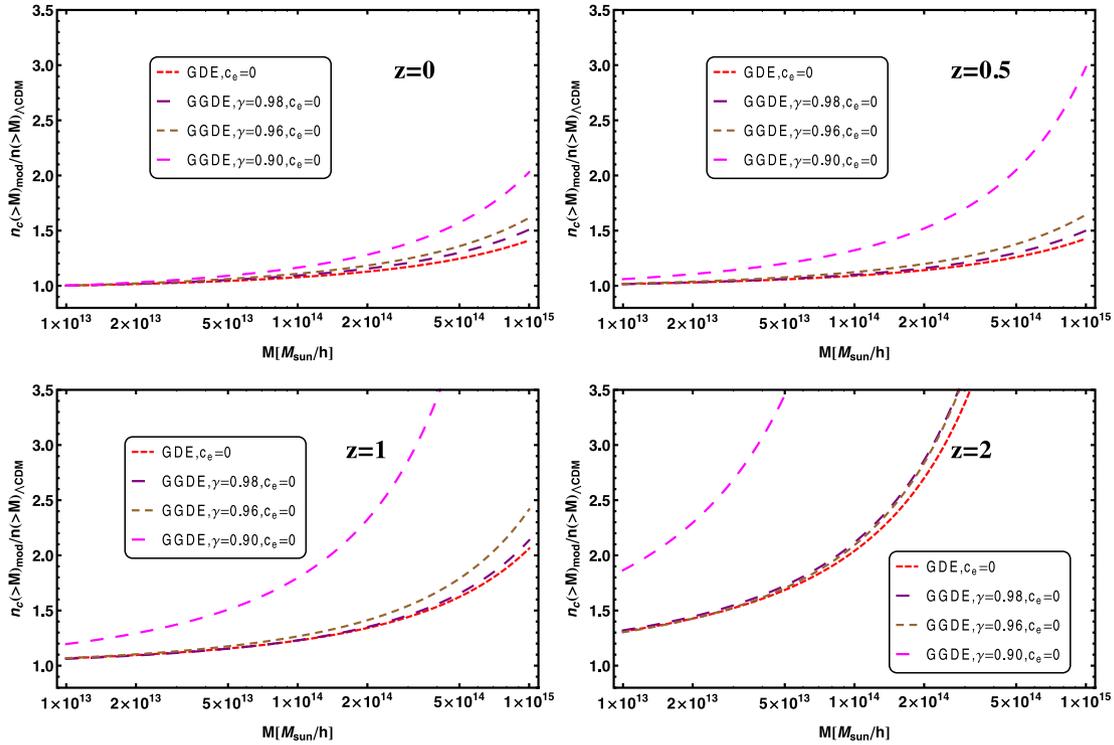
Figure 7. Ratio of the number of objects above a given mass M for haloes at $z = 0$ (top-left panel), $z = 0.5$ (top-right panel), $z = 1.0$ (bottom-left panel) and $z = 2.0$ (bottom-right panel) between the ghost and generalized ghost DE models and the concordance ΛCDM model by using the mass definition in equation (32). The red dot–dashed curve represents the clustering ghost DE model. The purple long-dashed, brown dashed and pink long-dashed curves stand for clustering generalized ghost DE model with model parameter $\gamma = 0.98$, 0.96 and 0.90, respectively.

DE perturbations, we change the mass of haloes as $M \rightarrow M(1 - \epsilon)$. In this case, the corrected mass function can be redefined as follows (Batista & Pace 2013):

$$\frac{\mathrm{d}n_c(z, M)}{\mathrm{d}M} = -\frac{\rho_{m0}}{M(1 - \epsilon)} \frac{\mathrm{d}\ln\sigma(M, z)}{\mathrm{d}M} f(\sigma), \qquad (34)$$

where $f(\sigma)$ is given by equation (26). It should be noted that the clustering of the DE component can also change the mass function $f(\sigma)$ by changing the quantities δ_c and $\sigma(M, z)$. In Fig. 7 we show the relative number density by using the corrected mass function formula in equation (34) and the definition of ϵ in equation (32). Analogously to Fig. 5, we choose four different redshifts $z = 0$, 0.5, 1 and $z = 2$. We see that due to the contribution of the DE mass, the relative number density between ghost and generalized DE models and ΛCDM model $n_c/n_{\Lambda \text{CDM}}$ is equal or larger than one. In the top panels, for $z = 0$ and 0.5, all ghost, generalized ghost and ΛCDM models generate the same number of objects at the low-mass end. However, at high masses, generalized ghost DE models with smaller value of the model parameter γ produce more objects. At higher redshifts, $z = 1$ and 2, one can see that ghost and generalized ghost DE models have more objects for both the low-mass and the high-mass tail compared to the concordance ΛCDM model. Comparing Figs 5 and 7, we conclude that for all the redshifts here considered, the predicted relative number density of haloes in the presence of DE corrections to the halo mass is higher than what was found for homogeneous DE scenarios. In particular, the differences are larger for high-mass objects. This feature of ghost and generalized ghost DE models is in agreement with the results of Batista & Pace (2013) for inhomogeneous early DE models. To compare the models quantitatively, we restrict our analysis to $z = 0$. While non-clustering DE models and the ΛCDM

model have the same number of objects (top-left panel of Fig. 5), clustering DE models deviate from the ΛCDM model particularly at the high-mass tail (top-left panel of Fig. 7). We see that clustering generalized ghost DE model with $\gamma = 0.90$ doubles the values obtained for the ΛCDM model, while for $\gamma = 0.96$ the increment in the number of objects is ≈ 61 per cent. Finally, for $\gamma = 0.98$, differences are of the order of 50 per cent. As expected, the increase in γ corresponds to a decrease in the differences with respect to the ΛCDM model at the high-mass tail (of the order of 40 per cent for the ghost DE model).

5 CONCLUSIONS

In this work, we studied the non-linear evolution of structure formation in ghost and generalized ghost DE models within the framework of the SCM. DE models are described by a constant or a time varying EoS $w(a)$ whose functional form is usually purely phenomenological. The advantage of dynamical DE models with respect to the ΛCDM model is that to alleviate its theoretical problems. Another interesting aspect is the presence of fluctuations in the DE fluid that can have an important and characteristic impact on non-linear structure formation. Ghost DE models are theoretically well motivated and trace their origin back to the studies of the low-energy effective QCD theory (Veneziano 1979; Witten 1979; Kawarabayashi & Ohta 1980; Rosenzweig et al. 1980). Here, we concentrate on the cosmological implications of such models and present results that can be useful from an observational point of view.

We start our analysis by studying the effects of the modification of the background expansion history of the growth factor and on a second step we take into account also the perturbations in the DE component. We showed that the linear growth factor is sensitive

to the details of the model considered. In particular, when DE is homogeneous, differences with respect to the ΛCDM model are very pronounced and can be up to 50 per cent at relatively high redshifts. Interestingly, when DE fluctuations are taken into account, differences become smaller and the models studied get closer to the ΛCDM model. This is exactly what happens for early DE model and it applies to this class of models as well, being the amount of DE at early times significantly more important (see bottom panel of Fig. 1).

Being the equations governing the evolution of the linearly extrapolated overdensity parameter δ_c identical to those of the linear growth factor, results are similar to what found for the linear growth factor. Once again when the perturbations in the DE fluid are included in the calculations, the models examined resemble closer the ΛCDM model. This is easily explained by taking into account that when DE perturbations play a role, Poisson equation is modified and this makes the model more similar to the ΛCDM one (see Batista & Pace 2013, for a more detailed discussion). Similar conclusions can be drawn for the non-linear virial overdensity Δ_V.

While the growth factor can be inferred from the determination of the matter power spectrum on linear scales at a given redshift or by measuring the quantity $f\sigma_8(z)$, where $f = \mathrm{d}\ln D_+/\mathrm{d}\ln a$ and $\sigma_8(z) = D_+(z)\sigma_8(z=0)$, the linear extrapolated overdensity δ_c is a purely theoretical quantity and it would be very hard to infer it from observations. Nevertheless they can be combined together and be the basic ingredients to evaluate the mass function and the number of haloes above a given mass. When keeping the DE fluid smooth and important only at the background level, we showed that both the ghost and generalized ghost models give an excess of objects with respect to the ΛCDM model, except for the generalized ghost model with lower value $\gamma = 0.9$. As expected, differences are very pronounced only for the high-mass tail of the mass function, while at low masses the models are practically indistinguishable.

One might consider that if DE can clump, then the total mass of the haloes should be affected. By defining the contribution of DE limited to that of the clumps, we showed in the top panel of Fig. 6 that the DE mass can be at least 10 per cent of the dark matter mass at $z = 0$, with differences growing with decreasing the parameter γ and decreasing at high redshift where the contribution of DE is less important. Note that if the amount of DE at early times is significantly bigger than in the ΛCDM model, then the DE mass can still be an appreciable fraction of the dark matter mass. By taking into account this correction and evaluating the number of objects above a given mass, we showed that the DE models we studied in this work predict much more objects with respect to the ΛCDM model at all redshifts. This could be a good test to compare theoretical predictions with observations.

REFERENCES

Abramo L. R., Batista R. C., Liberato L., Rosenfeld R., 2007, J. Cosmol. Astropart. Phys., 11, 12
Abramo L. R., Batista R. C., Liberato L., Rosenfeld R., 2008, Phys. Rev. D, 77, 067301
Abramo L. R., Batista R. C., Rosenfeld R., 2009a, J. Cosmol. Astropart. Phys., 7, 40
Abramo L. R., Batista R. C., Liberato L., Rosenfeld R., 2009b, Phys. Rev. D, 79, 023516
Appleby S. A., Linder E. V., Weller J., 2013, Phys. Rev. D, 88, 043526
Arkani-Hamed N., Creminelli P., Mukohyama S., Zaldarriaga M., 2004, J. Cosmol. Astropart. Phys., 4, 1
Armendariz-Picon C., Mukhanov V., Steinhardt P. J., 2000, Phys. Rev. Lett., 85, 4438
Armendariz-Picon C., Mukhanov V., Steinhardt P. J., 2001, Phys. Rev. D, 63, 103510
Ascasibar Y., Yepes G., Gottlöber S., Müller V., 2004, MNRAS, 352, 1109
Avila-Reese V., Firmani C., Hernández X., 1998, ApJ, 505, 37
Barkana R., Loeb A., 2001, Phys. Rep., 349, 125
Basse T., Eggers Bjælde O., Wong Y. Y. Y., 2011, J. Cosmol. Astropart. Phys., 10, 38
Batista R. C., Pace F., 2013, J. Cosmol. Astropart. Phys., 6, 44
Bertschinger E., 1985, ApJS, 58, 39
Bond J. R., Cole S., Efstathiou G., Kaiser N., 1991, ApJ, 379, 440
Bromm V., Yoshida N., 2011, ARA&A, 49, 373
Cai R.-G., 2007, Phys. Lett. B, 657, 228
Cai R.-G., Tuo Z.-L., Zhang H.-B., Su Q., 2011, Phys. Rev. D, 84, 123501
Cai R.-G., Tuo Z.-L., Wu Y.-B., Zhao Y.-Y., 2012, Phys. Rev. D, 86, 023511
Caldwell R. R., 2002, Phys. Lett. B, 545, 23
Carroll S. M., 2001, Living Rev. Relativ., 4, 1
Chiba T., Okabe T., Yamaguchi M., 2000, Phys. Rev. D, 62, 023511
Ciardi B., Ferrara A., 2005, Space Sci. Rev., 116, 625
Copeland E. J., Sami M., Tsujikawa S., 2006, Int. J. Mod. Phys. D, 15, 1753
Creminelli P., D'Amico G., Noreña J., Senatore L., Vernizzi F., 2010, J. Cosmol. Astropart. Phys., 3, 27
Del Popolo A., Pace F., Lima J. A. S., 2013a, Int. J. Mod. Phys. D, 22, 50038
Del Popolo A., Pace F., Maydanyuk S. P., Lima J. A. S., Jesus J. F., 2013b, Phys. Rev. D, 87, 043527
Del Popolo A., Pace F., Lima J. A. S., 2013c, MNRAS, 430, 628
Eisenstein D. J. et al., 2005, ApJ, 633, 560
Ferreira P. G., Joyce M., 1998, Phys. Rev. D, 58, 023503
Fillmore J. A., Goldreich P., 1984, ApJ, 281, 1
Gasperini M., Piazza F., Veneziano G., 2002, Phys. Rev. D, 65, 023508
Gunn J. E., Gott J. R., III, 1972, ApJ, 176, 1
Guth A. H., 1981, Phys. Rev. D, 23, 347
Ho S., Hirata C., Padmanabhan N., Seljak U., Bahcall N., 2008, Phys. Rev. D, 78, 043519
Hoffman Y., Shaham J., 1985, ApJ, 297, 16
Hořava P., Minic D., 2000, Phys. Rev. Lett., 85, 1610
Horellou C., Berge J., 2005, MNRAS, 360, 1393
Jaffe A. H. et al., 2001, Phys. Rev. Lett., 86, 3475
Jarosik N. et al., 2011, ApJS, 192, 14
Kawarabayashi K., Ohta N., 1980, Nucl. Phys. B, 175, 477
Komatsu E. et al., 2011, ApJS, 192, 18
Lahav O., Lilje P. B., Primack J. R., Rees M. J., 1991, MNRAS, 251, 128
Linde A., 1990, Phys. Lett. B, 238, 160
Maggiore M., Hollenstein L., Jaccard M., Mitsou E., 2011, Phys. Lett. B, 704, 102
Maor I., Lahav O., 2005, J. Cosmol. Astropart. Phys., 7, 3
Mehrabi A., Malekjani M., Pace F., 2015, Ap&SS, 356, 129
Mota D. F., van de Bruck C., 2004, A&A, 421, 71
Naderi T., Malekjani M., Pace F., 2015, MNRAS, 447, 1873
Nojiri S., Odintsov S. D., 2003a, Phys. Lett. B, 562, 147
Nojiri S., Odintsov S. D., 2003b, Phys. Lett. B, 565, 1
Ohta N., 2011, Phys. Lett. B, 695, 41
Pace F., Waizmann J.-C., Bartelmann M., 2010, MNRAS, 406, 1865
Pace F., Fedeli C., Moscardini L., Bartelmann M., 2012, MNRAS, 422, 1186
Pace F., Moscardini L., Crittenden R., Bartelmann M., Pettorino V., 2014a, MNRAS, 437, 547
Pace F., Batista R. C., Del Popolo A., 2014b, MNRAS, 445, 648
Padmanabhan T., 2002, Phys. Rev. D, 66, 021301
Padmanabhan T., 2003, Phys. Rep., 380, 235
Peacock J. A., 1999, Cosmological Physics. Cambridge Univ. Press, Cambridge
Peebles P. J. E., 1993, Principles of Physical Cosmology. Princeton Univ. Press, Princeton, NJ
Peebles P. J., Ratra B., 2003, Rev. Mod. Phys., 75, 559
Percival W. J. et al., 2010, MNRAS, 401, 2148
Perlmutter S. et al., 1999, ApJ, 517, 565
Piazza F., Tsujikawa S., 2004, J. Cosmol. Astropart. Phys., 7, 4
Planck Collaboration XV, 2014, A&A, 571, A15
Planck Collaboration XVI, 2014, A&A, 571, A16

Planck Collaboration XX, 2014, A&A, 571, A20
Press W. H., Schechter P., 1974, ApJ, 187, 425
Ratra B., Peebles P. J. E., 1988, Phys. Rev. D, 37, 3406
Riess A. G. et al., 1998, AJ, 116, 1009
Riess A. G. et al., 2004, ApJ, 607, 665
Riess A. G. et al., 2007, ApJ, 659, 98
Rosenzweig C., Schechter J., Trahern C. G., 1980, Phys. Rev. D, 21, 3388
Rozas-Fernández A., 2012, Phys. Lett. B, 709, 313
Ryden B. S., Gunn J. E., 1987, ApJ, 318, 15
Sahni V., Starobinsky A., 2000, Int. J. Mod. Phys. D, 9, 373
Sen A., 2002, J. High Energy Phys., 4, 48
Sheth R. K., Tormen G., 1999, MNRAS, 308, 119
Sheth R. K., Tormen G., 2002, MNRAS, 329, 61
Starobinsky A. A., 1980, Phys. Lett. B, 91, 99
Subramanian K., Cen R., Ostriker J. P., 2000, ApJ, 538, 528
Tegmark M. et al., 2004, Phys. Rev. D, 69, 103501
Thomas S., 2002, Phys. Rev. Lett., 89, 081301

Urban F. R., Zhitnitsky A. R., 2009a, J. Cosmol. Astropart. Phys., 9, 18
Urban F. R., Zhitnitsky A. R., 2009b, Phys. Rev. D, 80, 063001
Urban F. R., Zhitnitsky A. R., 2010a, Phys. Lett. B, 688, 9
Urban F. R., Zhitnitsky A. R., 2010b, Nucl. Phys. B, 835, 135
Veneziano G., 1979, Nucl. Phys. B, 159, 213
Wang L., Steinhardt P. J., 1998, ApJ, 508, 483
Wang Y., Tegmark M., 2005, Phys. Rev. D, 71, 103513
Weinberg S., 1989, Rev. Mod. Phys., 61, 1
Wetterich C., 1988, Nucl. Phys. B, 302, 668
White S. D. M., Rees M. J., 1978, MNRAS, 183, 341
Williams L. L. R., Babul A., Dalcanton J. J., 2004, ApJ, 604, 18
Witten E., 1979, Nucl. Phys. B, 156, 269
Zhitnitsky A. R., 2011, Phys. Rev. D, 84, 124008

This paper has been typeset from a TEX/LATEX file prepared by the author.